Published in final edited form as:
Biomaterials. 2014 August ; 35(26): 7346–7354. doi:10.1016/j.biomaterials.2014.05.014.

Tough and Flexible CNT-Polymeric Hybrid Scaffolds for Engineering Cardiac Constructs

Mahshid Kharaziha[a,b,1], **Su Ryon Shin**[a,b,c,1], **Mehdi Nikkhah**[a,b], **Seda Nur Topkaya**[a,b], **Nafiseh Masoumi**[a,b], **Nasim Annabi**[a,b,c], **Mehmet. R. Dokmeci**[a,b,c], and **Ali Khademhosseini**[a,b,c]

[a]Biomaterials Innovation Research Center, Division of Biomedical Engineering, Department of Medicine, Brigham and Woman's Hospital, Harvard, Medical School, Boston, MA, 02139, USA

[b]Harvard-MIT Division of Health Sciences and Technology, Massachusetts Institute of Technology, Cambridge, MA, 02139, USA

[c]Wyss Institute for Biologically Inspired Engineering, Harvard University, Boston, MA, 02115, USA

Abstract

In the past few years, a considerable amount of effort has been devoted toward the development of biomimetic scaffolds for cardiac tissue engineering. However, most of the previous scaffolds have been electrically insulating or lacked the structural and mechanical robustness to engineer cardiac tissue constructs with suitable electrophysiological functions. Here, we developed tough and flexible hybrid scaffolds with enhanced electrical properties composed of carbon nanotubes (CNTs) embedded aligned poly(glycerol sebacate):gelatin (PG) electrospun nanofibers. Incorporation of varying concentrations of CNTs from 0 to 1.5% within the PG nanofibrous scaffolds (CNT-PG scaffolds) notably enhanced fiber alignment and improved the electrical conductivity and toughness of the scaffolds while maintaining the viability, retention, alignment, and contractile activities of cardiomyocytes (CMs) seeded on the scaffolds. The resulting CNT-PG scaffolds resulted in stronger spontaneous and synchronous beating behavior (3.5-fold lower excitation threshold and 2.8-fold higher maximum capture rate) compared to those cultured on PG scaffold. Overall, our findings demonstrated that aligned CNT-PG scaffold exhibited superior mechanical properties with enhanced CM beating properties. It is envisioned that the proposed hybrid scaffolds can be useful for generating cardiac tissue constructs with improved organization and maturation.

Correspondence to: Ali Khademhosseini.

CORRESPONDING AUTHOR Ali Khademhosseini: alik@rics.bwh.harvard.edu.

[1]These authors equally contributed to this work.

Keywords

Cardiac tissue engineering; Scaffold; Cardiomyocyte; poly(glycerol sebacate):gelatin; Nanoparticles

1. Introduction

The extracellular matrix (ECM) of ventricular myocardium consists of protein-based nanofibrous networks (10 – 100 nm in diameter), which provide a soft and tough matrix to support cardiac cell functions [1]. Due to the inability of the heart to regenerate following myocardial infraction, there is an unmet need to engineer functional cardiac tissue constructs in vitro [2]. Recent advances in tissue engineering have paved the way to create cardiac grafts with relevant physiological characteristics similar to native myocardium. However, due to the complex architecture of myocardial tissue, there are still numerous challenges in developing fully functional and biomimetic cardiac substitutes.

In the past few years, synthetic and natural polymeric-based scaffolds have attracted considerable amount of attention for cardiac tissue engineering. These scaffolds have been mainly fabricated from polyurethane, elastin, poly(glycerol sebacate) (PGS), gelatin, alginate and their blends [3–9]. However, the majority of the previously reported scaffolds are electrically insulating at biologically relevant frequencies (heart muscles DC conductivity ~ 0.1 S/m) [10]. In addition, most of them have been morphologically and mechanically incompatible with the native myocardium ECM. Hydrogel-based scaffolds often lack the mechanical strength to support rigorous physiological loading conditions during cardiac cells' contraction cycles [11, 12]. Alternatively, stiff polymeric scaffolds have significantly hindered the contractility of the cardiac cells due to extreme stiffness of the matrix [13, 14]. To mimic the native myocardium, the scaffolds should exhibit suitable mechanical properties while providing sufficient flexibility to support the cyclic functions (i.e. contraction) [15]. Although microfabricated elastic scaffolds made of elastomeric polymers such as PGS have been previously developed to address these criteria, the microfabricated PGS scaffolds do not mimic the nanofibrous architecture of the native myocardium [7]. Therefore, a number of previous studies have focused on the development of nanofibrous scaffolds with tunable mechanical properties to recapitulate the architecture of the native myocardium ECM [9,16–18]. For instance, in our recent work, we developed highly aligned and elastic PGS:gelatin (PG) nanofibrous scaffolds through electrospinning process which were shown to promote the functionality of the cardiomyocytes (CMs) and cardiac fibroblasts (CFs) cultured on the scaffolds [9]. However, similar to most of the previous reports, these scaffolds did not provide electrically conductive matrices along with desired toughness (less than 270 kJm-3) [9].

To further improve the electrical and mechanical properties of the scaffolds, a number of studies have relied on the incorporation of conductive nanomaterials such as gold nanoparticles and carbon nanotubes (CNTs) within polymeric matrices for neural or cardiac tissue engineering applications [19, 20]. CNTs exhibit remarkable electrical and mechanical properties that make them of potential interest for tissue engineering applications [21–23].

For instance, in a recent study, CNTs were used to induce the differentiation of mesenchymal stem cells (MSCs) toward cardioprogenitor phenotype (or lineage) under electrical stimulation [24]. In another work, CNTs were employed to improve the mechanical properties of gelatin-based scaffolds for cardiac tissue engineering [8]. Despite improved physical and electrical properties, these scaffolds did not exhibit the desired toughness and architectural complexities suitable for cardiac tissue engineering.

In this work, we report on the development of aligned CNT-incorporated PG nanofibrous (CNT-PG) scaffolds for cardiac tissue engineering. It is hypothesized that the development of a tough and flexible nanofibrous scaffold with enhanced electrophysiological functionalities could simultaneously induce topographical, mechanical and electrical cues to support cardiac cell functions. We propose that the aligned CNT-PG nanofibrous scaffolds could potentially provide structural integrity to guide CMs alignment and enhanced electrical conductivity to achieve strong CM beating behavior.

2. Materials and Methods

2.1. Fabrication of CNT-PG hybrid nanofibrous scaffolds

CNT-PG scaffolds with various concentrations of CNTs were prepared by using electrospinning technique. Primarily, PG solution was prepared (PGS:gelatin of 1:2 weight ratio) in 80% acetic acid solution according to our previously reported procedure [9]. To obtain methacrylated gelatin (GelMA)-coated multi-walled CNTs, 25 mg of carboxyl acid group functionalized CNTs (NanoLab Inc, 30±15 nm in diameter, 5–20 μm in length, 95% purity) was added in 2% GelMA polymer solution and then sonicated for 1 hr (VCX 400, 80W, 2 sec on, 1 sec off) at room temperature to provide a homogenous dispersion of CNTs. To obtain various concentrations of CNT embedded polymer suspensions (0.05, 0.5 and 1.5%), a selected amount of sonicated stock suspension was added to PG solution and stirred in order to prepare a final homogenous suspension (“as prepared” polymer solution). To fabricate the nanofibrous scaffolds, “as prepared” polymer suspension fed into a standard syringe was electrospun at flow rate, voltage and the needle tip to the collector distance of 2 mL/h, 17 kV and 10 cm, respectively. A parallel electrode made of aluminum foil was used as a collector to create aligned nanofibrous scaffolds. Aligned and random PG and random 1.5% CNT-PG nanofibrous scaffolds were also fabricated as controls. Upon electrospinning, the fabricated scaffolds were vacuum-dried at room temperature overnight before the crosslinking process. A solution of N,N-(3-dimethylaminopropyl)-N'-ethyl-carbodiimide hydrochloride (EDC) and N-hydroxysuccinimide (NHS) (Sigma) in 90% ethanol was used to crosslink gelatin in the scaffolds. EDC concentration and the molar ratio of EDC/NHS were optimized at 75 mM and 2.5/1, respectively. After the crosslinking process, the uncrosslinked and excess EDC and NHS were removed by rinsing the scaffolds in DPBS solution.

2.2. Characterization of the hybrid nanofibrous scaffolds

Scanning electron microscopy (SEM, Philips, Germany) was used to visualize the structural topography of the uncrosslinked and crosslinked fibrous scaffold, which were sputter-coated with a thin layer of gold. The SEM images were applied in order to measure the average

fiber sizes (n=50), using (NIH) Image J software, and fiber orientation, using MATLAB program (MathWorks Inc., Natick, MA) within each scaffold. Fast Fourier Transform (FFT) analysis was used to quantify the fiber orientation according to previous procedures [7, 25]. Based on this analysis, the orientation index approached 90 degrees for random cell orientations; while for highly aligned cells, the orientation index approached zero [7]. Furthermore, CNTs distribution within the electrospun fibers was examined using transmission electron microscope (TEM) (Zeiss, Germany) on the samples directly collected on the carbon coated copper grid. The functional groups on the surface of the nanofibrous scaffolds were identified using a Senterra Raman spectroscope (Bruker, Germany) equipped with a 785 nm laser. For impedance analysis, the scaffolds were swollen in DPBS and then were punched between two gold sputter-coated glass slides and a.c. bias was swept over a frequency range from 40 Hz to 1.0 MHz (Solartron-1260A, United Kingdom). The impedance was subsequently recorded at each frequency [8].

The tensile properties of hydrated scaffolds with length: 8–10 mm, width: 6–8 mm, thickness: 0.10–0.25 mm were measured using a uniaxial tensile tester machine (Instron, Norwood, MA) with cell load capacity of 10 N at 7 mm/min rate. Before mechanical testing, the samples were soaked in Dulbecco's Phosphate buffered saline (DPBS) for 3 days at 37 °C. The stress–strain curves were plotted (n=5) and energy per volume (toughness), elastic modulus, ultimate tensile strength and strain at break (elongation) were obtained. The elastic modulus was calculated from the initial 0–10 % of linear region of the stress–strain curves while the energy per volume was measured from the area under the stress-strain curves.

In vitro degradation test was used to determine the weight loss of the crosslinked scaffolds (n=3) (length: 5 mm, width: 5 mm, thickness: 0.5 mm) incubated in DPBS at 37 °C for 1, 7, 14, 21 and 28 days. The samples were rinsed in DPBS, lyophilized using a freeze-dryer and weighted. The degradation percentage of each sample was calculated by dividing the weight loss to the initial dry weight.

2.3. Cell Culture

2.3.1. Rat cardiomyocytes isolation and culture—CMs were isolated from 2-day-old Sprague-Dawley rats according to a protocol accepted by the Institute's Committee on Animal Care [8]. Before cell seeding, crosslinked samples (n=3) attached on glass slides were sterilized in 70% ethanol for 30 min followed by UV light exposure for 30 min. The scaffolds with thickness of 100–250 μm were immersed in a cardiac medium composed of Dulbecco's modified eagle medium (DMEM) (Gibco, USA), 10% fetal bovine serum (FBS) (Gibco, USA), 1% L-Glutamine (Gibco, USA) and 100 units/ml penicillin-streptomycin (Gibco, USA) and were seeded with CMs (1.4×10^6 cells/cm^2).

2.3.2. The retention, viability and phenotype characterization of cultured cardiomyocytes—CM retention was quantified by counting the number of CMs adhered to the scaffolds after one day of seeding. Nuclei were stained with 1:1000 dilution of 4′,6-diamidino-2-phenyl indole dihydrochloride (DAPI) stain (Invitrogen) in DPBS (5 min, room temperature) for visualization. One day after cell seeding, the samples were fixed (30 min, room temperature) in 4% paraformaldehyde (PF) solution in DPBS and stained with DAPI.

Fluorescent images taken from 10 regions of each sample (n=3) using an inverted microscope (Nikon TE 2000-U, Nikon instruments Inc., USA) were analyzed by Image J software in order to count the number of cells per unit area.

CM viability was determined using a Live/Dead assay kit (calcein-AM/ethidium Bromide homodimer, Invitrogen) according to the manufacturer's instructions. Ten selected areas within each sample (n=3) were imaged using fluorescence microscope and subsequently cell viability was measured using Image J software based on counting the number of live and dead cells. Metabolic activity of CMs seeded on the scaffolds (n=3) was determined using Alamar Blue (AB) assay (Invitrogen) at days 0, 4 and 7 of culture according to the manufacturer's protocols.

Immunocytochemistry of CMs markers was performed after 7 days of culture for cardiac-specific proteins including sarcomeric α-actinin, connexin-43 (Cx43) and troponin I. To perform immunostaining, CMs seeded on the scaffolds were fixed in 4% PF in DBPS for 30 min at room temperature) and permeabilized with 0.1% Triton X-100 for 30 min at room temperature. Then, the samples blocked in 10% goat serum (GS) were soaked (4 °C, 24 h) in 1:200 dilution of primary antibodies specific to sarcomeric α-actinin, Cx43 and troponin I in 10% GS. The sample were subsequently treated with secondary antibodies (1:200 dilution) consisting of Alexa Fluor-488 conjugated goat anti-mouse antibody for sarcomeric α-actinin, Alexa Fluor-594 goat anti-mouse for troponin I, and Alexa Fluor-594 goat anti-rabbit for Cx43 in 10% GS for 40 min at room temperature). Finally, the nuclei were stained with 1:1000 dilution of DAPI stain in DPBS for 5 min. The fluorescence images were taken from samples and then analyzed using image J software. Finally, the cellular alignment was quantified according to previously described procedures [26] using DAPI-stained cells nuclei at six different locations of each sample (Cell number: 500–1000).

2.3.3. Characterization of the contractile behavior of cultured cardiomyocytes

—The contractile behavior of CMs cultured on the scaffolds, with and without electrical stimulation (spontaneous beating), was investigated through monitoring their beating activity. Beating videos were obtained using a microscope equipped with a temperature control chamber at 37 °C and a CCD camera. The number of beats per min (BPM) of CMs was measured using video-recorded beating sequences digitized at a rate of 20 frames per second by a custom written MATLAB program [27]. The BPM was measured at three different points within each scaffold.

In addition to spontaneous beating analysis, electrical stimulation was used to precisely evaluate the effects of CNT concentration on the CMs contractile behavior. Electric field stimulation was performed at day 7 of culture using a modified carbon electrode set up according to previously established protocols [9]. The scaffolds were placed in culture medium between two-carbon electrode rods (1 cm spacing) connected to an electrical stimulator and an oscilloscope to measure the output signals. Biphasic square waveforms with 50 ms pulses were applied at amplitude of 0–7 V/cm and frequency of 1–3 Hz. Stimulation excitation threshold (ET) and maximum capture rate (MCR) were also determined according to the minimum voltage for synchronous beating of CMs and the maximum pacing frequency recognized at ET, respectively.

2.4. Statistical Analysis

Statistical analysis was measured by one-way ANOVA analysis followed by Tukey's post-hoc test using GraphPad Prism Software (V.5). Data was reported as mean ± standard deviation (SD). A *P*-value < 0.05 was taken to be significant.

3. Results and discussion

3.1. Fabrication and characterization of the hybrid nanofibrous scaffolds

Native ventricular myocardium consists of nanofibrous collagen-based ECM and electrically conductive purkinje fibers. Such unique architecture maintains aligned and elongated tissue structure and enables electrical signal propagation along the cardiac cells, which ultimately facilitates strong synchronous contractions of the tissue [28]. In order to mimic the native myocardium ECM, aligned CNT-PG scaffolds were fabricated using electrospinning (Fig. 1A and Fig. S1A). SEM images (Fig. 1B, C) demonstrated successful fabrication of the aligned 1.5% CNT-PG scaffold (1.5% CNT-PG) with highly uniform morphology. The average fiber size of 1.5% CNT-PG scaffold was in the range of 167±82 nm (Fig. S1B). Compared to other CNTs incorporated scaffolds and the control group (random 1.5% CNT-PG scaffold), the smaller fiber sizes of the scaffolds as a result of increased CNT concentration might be due to higher conductivity of the pre-polymer solution. In particular, the conductivity of the polymeric solution provided a stronger electrical force in the electrospinning process leading to the enhanced elongation and decreased fiber size [29]. Moreover, TEM analysis showed individual CNTs (25±12 nm in diameter) in parallel orientation within the nanofibers axis (Fig. 1D). Therefore, it was confirmed that during the fabrication process, randomly distributed CNTs within the pre-polymer solution were well dispersed and ultimately aligned along the nanofibers axis due to the uniaxial direction of the fluid jet [30, 31]. The successful dispersion of CNTs was due to their bio-functionalization through coating with GelMA polypeptide chains. The CNT surfaces are highly hydrophobic, which usually results in precipitation and aggregation in biological media or polymer solution [32]. However, the interaction between the polymeric chains and the surface of CNTs has been shown to be an effective way to coat and separate nanotubes within the polymeric solution [33]. Our previous findings also confirmed that a thin layer of GelMA could be uniformly coated on the CNT surfaces due to the hydrophobic interactions between the polypeptide chain and the CNT sidewalls [34]. A critical issue during the dispersion of CNTs into the prepolymer solution is the introduction of structural defects on CNTs leading to reduced electrical and mechanical properties of the composite scaffolds [34]. In Raman spectra of the pure CNT and CNT-PG scaffold (Fig. 1E), the ratio between the G-band and D-band [34] of CNTs, observed at 1609 cm^{-1} and 1300 cm^{-1} respectively, was similar to those from bare CNTs and composites. Therefore, the short sonication time (~ 1 hr) led to well dispersion of CNTs in the polymeric matrix with minimal structural damage, which improved the mechanical properties of hybrid scaffolds.

To stabilize the structure of nanofibrous scaffolds in biological media, gelatin was chemically crosslinked using EDC/NHS crosslinking agents according to our previously reported method [9]. SEM images of crosslinked scaffolds (Fig. 1F and Fig. S2) revealed the alterations in the morphology of scaffolds (increased average fiber diameter), which was due

to the swelling of the nanofibers through the crosslinking process. Such observations agreed well with our previous study conducted on PG scaffolds [9]. Additionally, similar to uncrosslinked versions, the average fiber sizes of the scaffolds significantly reduced through increasing the CNTs concentration (Fig. 1G). In particular, the average fiber diameter of the crosslinked 1.5% CNT-PG scaffold was in the range of 210±91 nm. While the average fiber size of 1.5% CNT-PG scaffold did not show any significant differences compared to random 1.5% CNT-PG scaffold (control), and it was smaller than those made of pure PG (280±56 nm). We evaluated the alignment degree of CNT-PG hybrid scaffolds as the key architectural factor affecting the organization of the cardiac cells. Fiber orientation was quantified by the Fast Fourier Transform (FFT)-based analysis technique using SEM images (Fig. 1F and Fig. S2A). The FFT analysis was performed to obtain the fraction curves from SEM images. The orientation index was calculated by measuring angular increment, encompassing 50% of the total area under the fraction curve centered at the angle of highest frequency (Fig. S2B). The lower orientation index indicated a narrower mean distribution and more parallel fibers as shown in Fig. 1H. Our results showed that the orientation index of 1.5% CNT-PG was significantly lower than that of other scaffolds. This could be as a result of enhanced molecular orientation of the composite matrix, mainly due to the fact that the CNTs acted as nucleating sites for the formation of oriented crystallites. These results are consistent with the previous studies on other polymeric matrices such as poly (vinyl alcohol) (PVA) and polyaniline [35–37]. Such orientation index values (Fig. 1H) of the developed scaffolds are expected to enhance the alignment of cardiac cells. Notably, the orientation index value of 1.5% CNT-PG (38±4°) closely mimicked the adult rat right ventricular myocardium (~40°) [7], confirming that these scaffolds can be used as a suitable matrix to recapitulate the aligned structure of the native myocardium ECM.

The highly aligned CNT-PG scaffolds exhibited robust mechanical properties along with controlled flexibility (Fig. 2A). To evaluate the effects of CNTs on the mechanical properties of PG scaffolds, uniaxial tensile tests were performed on the scaffolds, submerged in DPBS. The stress-strain curves of the fabricated scaffolds (Fig. 2B) indicated that their mechanical properties were significantly modulated by the addition of CNTs. In particular, incorporation of 1.5% CNTs significantly enhanced the toughness, tensile strength and elastic modulus of scaffolds by 7-, 5.9- and 4-fold, respectively, compared to PG scaffolds. However, the elongation of the hybrid scaffolds was close to that of the PG scaffold (Supplementary Table S1). The enhanced mechanical properties of the CNT-PG hybrid scaffolds might be due to the orientation of CNTs along the preferred axis of the fibers as well as the strong interaction between CNTs and the polymeric matrix [38]. As depicted in Fig. 1A, the carboxylic (COOH) and the amide (NH_2) groups of GelMA coated CNTs and gelatin crosslinked after treatment with EDC/NHS. These strong interactions are expected to be the main mechanism, which efficiently transfers the mechanical stress from the polymer matrix to CNTs, leading to higher stiffness and tensile strength. Additionally, the improved toughness of scaffolds (1948.7±156 KJm^{-3}) is attributed to higher energy absorption during the loading condition due to slippage at the CNT-polymer matrix interface [39]. Therefore, a superior property of the developed hybrid scaffolds is their high toughness as compared to previously reported nanofibrous scaffolds (Fig. 2(C)) [18, 23, 40–46]. To name a few examples, the toughness and elastic modulus of CNT incorporated PVA fibrous scaffolds

were about 228 KJm^{-3} and 158 kPa, respectively [40], which were significantly lower than the values obtained for 1.5% CNT-PG scaffold (1948.7±156 KJm^{-3} and 373.5±47 kPa).

With respect to the electrical properties of the scaffolds, conductivity of the hybrid scaffolds was enhanced through the incorporation of CNTs. Due to the capacitive currents at high frequencies (>10 kHz), all scaffolds revealed low impedance values (Fig. 2D). At physiologically relevant frequencies (below 0.1 kHz), the impedance of CNT-PG was lower than PG scaffold. Degradation of fibrous scaffolds is usually dependent on their chemical and physical (i.e. fiber diameter, pore size, and porosity) properties. The average fiber diameter of CNT-PG scaffolds was smaller than that of pristine PG. The incorporation of CNTs reduced the degradation rate of CNT-PG scaffolds compared to that of pristine PG (Fig. S3). Therefore, the degradation rates of the scaffolds could be precisely tuned by varying the concentration of CNTs attributed to the strong binding between the CNTs and the PG matrix. Previous reports have shown that conductive scaffolds facilitate maturation of CMs and improve beating propagation among CMs compared to insulating polymer [5,10,47]. However, most of these conductive scaffolds lacked aligned nanofibrous architectures to regulate essential cellular functions such as morphogenesis. The engineered conductive construct in our study supported CM alignment in the direction of aligned fibers presented within the 3D structure of the scaffold. Our results suggest that the CNT-PG hybrid scaffolds have the potential to be useful for engineering myocardium tissue due to its high toughness, enhanced conductivity, anisotropic structure, and proper degradation profile.

3.2. Organization of cardiomyocytes cultured on the hybrid nanofibrous scaffolds

As native myocardium is exposed to large and continuous mechanical stresses, high level of toughness is required to avoid matrix failure during tissue contraction [48]. Furthermore, since an extremely stiff matrix (elastic modulus > 0.8 MPa) [13, 14], inhibits the maturation and contractile properties of cardiac cells, engineered matrices should be relatively elastic (similar to native tissue ~ 54–240 kPa [7]) to provide a suitable microenvironment for the contractile activities of cardiac cells [49]. To investigate the suitability of the developed tough CNT-PG scaffolds in supporting cardiac cells functions, CMs were seeded on the CNT-PG scaffolds. Cell attachment, viability and proliferation were then investigated over a period of 7 days of culture. Phase contrast images after one day of culture (Fig. 3A) indicated that CMs homogenously distributed and grew on both PG and CNT-PG scaffolds. However, cell retention on CNT-PG scaffolds was significantly higher than those of pure PG scaffold (Fig. 3B). Such behavior could be due to smaller fiber diameter and higher surface-to-volume ratios, which enhanced ECM protein adsorption [50]. Live/dead assay indicated high percentage of viable cells after one day of culture (upon 89±5%). In fact, CNT-PG hybrid scaffolds significantly increased CM viability as compared to the PG scaffold (Fig. 3C and Supplementary Fig. S4). Consistent with our findings, previous studies also reported higher cellular attachment and retention on CNT embedded GelMA hybrid hydrogel scaffolds compared to pure GelMA due to increased stiffness of the matrix through incorporation of CNTs [34]. In addition, cardiac cells exhibited higher metabolic activities on the CNT-PG hybrids compared to the PG scaffold after 4 and 7 days of culture (Fig. 3D). As the neonatal rat cardiac isolation contains immature CMs along with CFs [51], significantly enhanced cellular proliferations might be due to the proliferative capacity of

CFs seeded along with CMs on the scaffolds. Considering that CFs metabolic activity was previously shown to vary as a function of chemical and mechanical properties of the scaffolds [9], the increased CFs metabolic activity could be due to the higher stiffness of the CNT-PG hybrid scaffolds as compared to the PG scaffold. Therefore, CNTs promoted cell retention, viability, proliferation without inducing cytotoxicity during the 7 days of culture.

It is well known that the topographical cues within the matrix play a crucial role in regulating cells morphology [52]. In our study, CMs were able to sense the underlying topography and progressively align along the fiber direction quantified through the alignment of cellular nuclei (Fig. 3E). In particular, distribution of cells' nuclei alignment at day 7 of culture on different scaffolds (Fig. 3E, F) revealed that on 1.5% CNT-PG scaffolds, CMs exhibited significantly higher alignment (~72% within 0–10 degree preferred angle) compared to PG (~55%) and random 1.5% CNT-PG scaffolds (control). Due to the anisotropy of the aligned nanofibrous scaffolds, the traction forces exerted by filopodia were mainly guided in the direction of the fibers axis, ultimately leading to the alignment and organization of the CMs [53]. The different degrees of cellular organization on the aligned nanofibrous scaffolds are likely due to the coupled effects of structural, chemical and mechanical cues of the scaffolds [9]. This assumption is supported by our previous results in Fig. 1G, Fig. 1H, and Fig. 2B. The fiber size (Fig. 1G), orientation index (Fig. 1H), elastic modulus (Fig. 2B), and cell retention (Fig. 3B) with varied CNT concentrations followed the same trend as the alignment of CMs on the scaffolds. These results suggest that cell binding, mechanical stiffness, and topographical factor play an important role in regulating cellular organizations. Thus, we can infer that CNT incorporated aligned nanofibrous scaffolds promoted the organizations of CMs by resembling the physical features of nanofibrous collagen-based ECM.

3.3. Expression of cardiac markers of cardiomyocytes cultured on hybrid nanofibrous scaffolds

The effects of CNTs and the scaffold architecture on the maturation of CMs were also assessed using immunofluorescence staining for specific cardiac markers including contractile protein sarcomeric α-actinin, calcium binding troponin I, and cardiac gap junction protein Cx43 (Fig. 3G, H and Fig. S5). The sarcomeric α-actinin is a crucial marker for strong contractility and maturation of CMs [2]. Immunofluorescence staining demonstrated that cardiac tissue cultured on 1.5% CNT-PG and PG scaffolds exhibited well-developed interconnected sarcomeric structures. However, the alignment of sarcomeres along the major direction of nanofibers was more pronounced on the 1.5% CNT-PG compared to the PG scaffold (Fig. 3G). Additionally, as a result of multiple overlapping cross-striations, cardiac tissue constructs did not exhibit any preferred orientation on the random CNT-PG and PG scaffolds (Fig. S5A). CMs exhibited higher expression and uniform distribution of Cx43 (responsible marker for cell-cell communication, regulating electrical and mechanical junctions [54]) on the 1.5% CNT-PG scaffolds as compared to PG and random 1.5% CNT-PG scaffolds, indicating enhanced cell-cell coupling and improved contractile properties (Figs. 3G and S5A). The expression of troponin I, a marker involved in muscle calcium binding, cytoskeletal organization and cellular contraction [55], was similar for the tissues developed on the aligned and random 1.5% CNT-PG and PG

scaffolds. However, on the random scaffolds, troponin I was less organized with fewer connections compared to the aligned scaffolds (Fig. S5B). Our findings demonstrated that aligned nanofibrous scaffolds enhanced CM maturation in comparison to random ones.

3.4. Beating behavior of the engineered cardiac tissue

All the cardiac tissues cultured on the developed scaffolds started spontaneous synchronous beating only after one day of culture and demonstrated enhanced beating rate during 5 days of culture (Fig. 4A). The CM beating rate (beats/min (BPM)) on the CNT-PG scaffolds was significantly higher than those on the PG scaffold (i.e. 98.5 ± 6.2 BPM on 1.5% CNT-PG hybrid compared to 47.2 ± 8.5 BPM on PG scaffold on day 5). In addition, the beating rate of CMs on the CNT-PG scaffolds did not appear to be significantly altered as a function of CNT concentrations. However, the beating rate of cardiac cells cultured on CNT-PG scaffolds was consistent with strong and synchronized beating behavior as the concentration of CNTs was increased (Fig. 4B, C and Supplementary Video S1). This could be due to the enhanced cellular alignment, higher flexibility and toughness of scaffolds and higher expression of cardiac markers on CNT-PG scaffolds (Fig. 3E, G and 4C). While aligned tissue sheets were formed on both PG and 1.5% CNT-PG scaffolds (Fig. 4C), the uniformity of the engineered tissue constructs was more pronounced on the 1.5% CNT-PG scaffolds (the red arrows showed uneven distribution of CMs on PG compared to 1.5% CNT-PG).

The effect of CNTs on beating behavior of the cardiac tissues was also estimated through electrical excitability of the tissue. Electrical stimulation markedly enhanced the contraction of the tissues on PG and CNT-PG scaffolds observed through stronger and synchronous beating patterns (Supplementary Video S2 and Fig. 4D). The excitation threshold (ET) indicating the minimum voltage which induced synchronized beating at each frequency, was the lowest on the 1.5% CNT-PG scaffold (2.0 ± 1.0 V, at 3 Hz), which followed an increasing trend (4-fold) by decreasing the CNT content to 7.0 ± 1.0 V (at 3 Hz) on PG scaffolds (Fig. 4E). Furthermore, the maximum capture rate (MCR), indicating the contractile versatility of the CMs and their ability to beat at high frequencies, was highest on the 1.5% CNT-PG scaffold (Fig. 4F). Within the random 1.5% CNT-PG scaffold (control), ET and MCR were significantly higher and lower, respectively, compared to aligned CNT-PG and PG scaffolds. These results suggest the positive correlation of CM attachment and organization on the aligned scaffolds with the electrical excitability of the engineered tissue construct. Similar findings were also reported for CNT-GelMA scaffolds confirming higher CM attachment, organization and spontaneous synchronous beating (about 3-fold) and lower excitation threshold compared to pure GelMA hydrogels [8]. Taken altogether, our findings indicated that simultaneously enhanced toughness and electrical properties of CNT-PG hybrid scaffolds along with their highly organized architectures promoted CM viability, retention, alignment, maturation, and function. Furthermore, increasing CNT concentrations up to 1.5% resulted in the formation of a more homogeneous cardiac tissue construct with strong contractile properties.

4. Conclusion

In summary, GelMA-coated CNTs were successfully incorporated within PG nanofibrous scaffolds using an electrospinning process. Physical interactions between CNTs and the PG matrix enabled homogeneous dispersion of CNTs in the scaffolds and resulted in significantly improved electrical and mechanical properties. Notably, incorporation of 1.5% CNTs enhanced the toughness of the scaffolds by 7-fold while elongation did not significantly change. Increasing the CNT content resulted in enhanced fiber orientation, mimicking the anisotropic structure of left ventricular myocardium. The alignment of CMs was mainly affected by the architecture of the scaffolds and enhanced as a function of CNT concentrations. In addition, the contractile properties of the CMs were significantly improved through incorporation of CNTs. The aligned nanofibrous architecture along with enhanced electrical conductivity and toughness of the CNT-PG scaffolds provides a suitable matrix to support cardiac cell functions. The developed hybrid scaffolds can be potentially used as a graft for cardiac or neuron tissue constructs. In our future work, we aim to stack these layers and create a complex thick tissue incorporated with vascular networks for delivery of nutrients. Therefore, this CNT polymeric hybrid scaffold can be useful for *in vitro* cell studies or fabricating complex biomimetic tissue-like structures for organs-on-a-chip applications and drug studies.

Supplementary Material

Refer to Web version on PubMed Central for supplementary material.

Acknowledgments

The authors acknowledge funding from the Presidential Early Career Award for Scientists and Engineers (PECASE), the Office of Naval Research Young National Investigator Award, the National Science Foundation CAREER Award (DMR 0847287), and the National Institutes of Health (HL092836, AR057837, DE021468, DE019024, EB012597, HL099073, EB008392).

References

1. Chien KR, Domian IJ, Parker KK. Cardiogenesis and the complex Biology of regenerative cardiovascular Medicine. Science. 2008; 322:1494–1497. [PubMed: 19056974]
2. Tandon V, Zhang B, Radisic M, Murthy SK. Generation of tissue constructs for cardiovascular regenerative medicine: From cell procurement to scaffold design. Biotechnol Adv. 2013; 31:722–735. [PubMed: 22951918]
3. Rockwood DN, Akins RE Jr. Parrag IC, Woodhouse KA, Rabolt JF. Culture on electrospun polyurethane scaffolds decreases atrial natriuretic peptide expression by cardiomyocytes in vitro. Biomaterials. 2008; 29:4783–4791. [PubMed: 18823659]
4. Annabi N, Tsang K, Mithieux SM, Nikkhah M, Ameri A, Khademhosseini A, et al. Highly elastic micropatterned hydrogel for engineering functional cardiac tissue. Adv Funct Mater. 2013; 23:4950–4959.
5. Dvir T, Timko BP, Brigham MD, Naik SR, Karajanagi SS, Levy O, et al. Nanowired three-dimensional cardiac patches. Nat Nanotechnol. 2011; 6:720–725. [PubMed: 21946708]
6. Murtuza B, Nichol JW, Khademhosseini A. Micro- and nanoscale control of the cardiac stem cell niche for tissue fabrication. Tissue Eng Part B Rev. 2009; 15:443–454. [PubMed: 19552604]
7. Engelmayr GC Jr. Cheng M, Bettinger CJ, Borenstein JT, Langer R, Freed LE. Accordionlike honeycombs for tissue engineering of cardiac anisotropy. Nat Mater. 2008; 7:1003–1010. [PubMed: 18978786]

8. Shin SR, Jung SM, Zalabany M, Kim K, Zorlutuna P, Kim SB, et al. Carbon-nanotube-embedded hydrogel sheets for engineering cardiac constructs and bioactuators. ACS Nano. 2013; 7:2369–2380. [PubMed: 23363247]
9. Kharaziha M, Nikkhah M, Shin S-R, Annabi N, Masoumi N, Gaharwar AK, et al. PGS:Gelatin nanofibrous scaffolds with tunable mechanical and structural properties for engineering cardiac tissues. Biomaterials. 2013; 34:6355–6366. [PubMed: 23747008]
10. You J-O, Rafat M, Ye GJC, Auguste DT. Nanoengineering the heart: conductive scaffolds enhance connexin 43 expression. Nano Lett. 2011; 11:3643–3648. [PubMed: 21800912]
11. Zimmermann WH, Melnychenko I, Wasmeier G, Didie M, Naito H, Nixdorff U, et al. Engineered heart tissue grafts improve systolic and diastolic function in infarcted rat hearts. Nat Med. 2006; 12:452–458. [PubMed: 16582915]
12. Feng Z, Matsumoto T, Nakamura T. Measurements of the mechanical properties of contracted collagen gels populated with rat fibroblasts or cardiomyocytes. J Artif Organs. 2003; 6:192–196. [PubMed: 14598103]
13. Forte G, Pagliari S, Ebara M, Uto K, Van Tam JK, Romanazzo S, et al. Substrate stiffness modulates gene expression and phenotype in neonatal cardiomyocytes in vitro. Tissue Eng Part A. 2012; 18:1837–1848. [PubMed: 22519549]
14. Gupta MK, Walthall JM, Venkataraman R, Crowder SW, Jung DK, Yu SS, et al. Combinatorial polymer electrospun matrices promote physiologically-relevant cardiomyogenic stem cell differentiation. Plos One. 2011; 6:e28935. [PubMed: 22216144]
15. Papadaki M, Bursac N, Langer R, Merok J, Vunjak-Novakovic G, Freed LE. Tissue engineering of functional cardiac muscle: molecular, structural, and electrophysiological studies. Am J Physiol Heart Circ Physiol. 2001; 280:H168–H178. [PubMed: 11123231]
16. Dvir T, Timko BP, Kohane DS, Langer R. Nanotechnological strategies for engineering complex tissues. Nat Nanotechnol. 2011; 6:13–22. [PubMed: 21151110]
17. Zong XH, Bien H, Chung CY, Yin LH, Fang DF, Hsiao BS, et al. Electrospun fine-textured scaffolds for heart tissue constructs. Biomaterials. 2005; 26:5330–5338. [PubMed: 15814131]
18. Mukherjee S, Venugopal JR, Ravichandran R, Ramakrishna S, Raghunath M. Evaluation of the Biocompatibility of PLACL/Collagen Nanostructured Matrices with Cardiomyocytes as a Model for the Regeneration of Infarcted Myocardium. Adv Funct Mater. 2011; 21:2291–2300.
19. Lovat V, Pantarotto D, Lagostena L, Cacciari B, Grandolfo M, Righi M, et al. Carbon nanotube substrates boost neuronal electrical signaling. Nano Lett. 2005; 5:1107–1110. [PubMed: 15943451]
20. Zhou J, Chen J, Sun H, Qiu X, Mou Y, Liu Z, et al. Engineering the heart: Evaluation of conductive nanomaterials for improving implant integration and cardiac function. Sci Rep. 2014; 4:3733. [PubMed: 24429673]
21. Polizu S, Savadogo O, Poulin P, Yahia LH. Applications of carbon nanotubes-based biomaterials in biomedical nanotechnology. J Nanosci Nanotechnol. 2006; 6:1883–1904. [PubMed: 17025102]
22. Menard-Moyon C, Kostarelos K, Prato M, Bianco A. Functionalized carbon nanotubes for probing and modulating molecular functions. Chem Biol. 2010; 17:107–115. [PubMed: 20189101]
23. Lee CK, Shin SR, Mun JY, Han S-S, So I, Jeon J-H, et al. Tough Supersoft Sponge Fibers with Tunable Stiffness from a DNA Self-Assembly Technique. Angew Chem Int Ed Engl. 2009; 48:5116–5120. [PubMed: 19263454]
24. Mooney E, Mackle JN, Blond DJP, O'Cearbhaill E, Shaw G, Blau WJ, et al. The electrical stimulation of carbon nanotubes to provide a cardiomimetic cue to MSCs. Biomaterials. 2012; 33:6132–6139. [PubMed: 22681974]
25. Ayres C, Bowlin GL, Henderson SC, Taylor L, Shultz J, Alexander J, et al. Modulation of anisotropy in electrospun tissue-engineering scaffolds: Analysis of fiber alignment by the fast Fourier transform. Biomaterials. 2006; 27:5524–5534. [PubMed: 16859744]
26. Nikkhah M, Eshak N, Zorlutuna P, Annabi N, Castello M, Kim K, et al. Directed endothelial cell morphogenesis in micropatterned gelatin methacrylate hydrogels. Biomaterials. 2012; 33:9009–9018. [PubMed: 23018132]

27. Kim SB, Bae H, Cha JM, Moon SJ, Dokmeci MR, Cropek DM, et al. A cell-based biosensor for real-time detection of cardiotoxicity using lensfree imaging. Lab Chip. 2011; 11:1801–1807. [PubMed: 21483937]
28. Fleischer S, Dvir T. Tissue engineering on the nanoscale: lessons from the heart. Curr Opin Biotechnol. 2013; 24:664–671. [PubMed: 23142543]
29. Reneker DH, Chun I. Nanometre diameter fibres of polymer, produced by electrospinning. Nanotechnol. 1996; 7:216–223.
30. Ko F, Gogotsi Y, Ali A, Naguib N, Ye HH, Yang GL, et al. Electrospinning of continuous carbon nanotube-filled nanofiber yarns. Adv Mater. 2003; 15:1161–1165.
31. Salalha W, Dror Y, Khalfin RL, Cohen Y, Yarin AL, Zussman E. Single-walled carbon nanotubes embedded in oriented polymeric nanofibers by electrospinning. Langmuir. 2004; 20:9852–9855. [PubMed: 15491224]
32. Zheng W, Zheng YF. Gelatin-functionalized carbon nanotubes for the bioelectrochemistry of hemoglobin. Electrochem Commun. 2007; 9:1619–1623.
33. Liu Y, Liu X, Wang X. Biomimetic synthesis of gelatin polypeptide-assisted noble-metal nanoparticles and their interaction study. Nanoscale Res Lett. 2011; 6:22.
34. Shin SR, Bae H, Cha JM, Mun JY, Chen Y-C, Tekin H, et al. Carbon Nanotube Reinforced Hybrid Microgels as Scaffold Materials for Cell Encapsulation. ACS Nano. 2012; 6:362–372. [PubMed: 22117858]
35. Zhang Y, Rutledge GC. Electrical conductivity of electrospun polyaniline and polyaniline-blend fibers and mats. Macromolecules. 2012; 45:4238–4246.
36. Minus ML, Chae HG, Kumar S. Interfacial Crystallization in Gel-Spun Poly(vinyl alcohol)/Single-Wall Carbon Nanotube Composite Fibers. Macromol Chem Phys. 2009; 210:1799–1808.
37. Song K, Zhang Y, Meng J, Green EC, Tajaddod N, Li H, et al. Structural Polymer-Based Carbon Nanotube Composite Fibers: Understanding the Processing-Structure-Performance Relationship. Materials. 2013; 6:2543–2577.
38. Spinks GM, Shin SR, Wallace GG, Whitten PG, Kim SI, Kim SJ. Mechanical properties of chitosan/CNT microfibers obtained with improved dispersion. Sens Actuators B Chem. 2006; 115:678–684.
39. Salvetat-Delmotte JP, Rubio A. Mechanical properties of carbon nanotubes: a fiber digest for beginners. Carbon. 2002; 40:1729–1734.
40. Liao H, Qi R, Shen M, Cao X, Guo R, Zhang Y, et al. Improved cellular response on multiwalled carbon nanotube-incorporated electrospun polyvinyl alcohol/chitosan nanofibrous scaffolds. Colloids Surf B Biointerfaces. 2011; 84:528–535. [PubMed: 21353768]
41. Daamen WF, van Moerkerk HTB, Hafmans T, Buttafoco L, Poot AA, Veerkamp JH, et al. Preparation and evaluation of molecularly-defined collagen-elastin-glycosaminoglycan scaffolds for tissue engineering. Biomaterials. 2003; 24:4001–4009. [PubMed: 12834595]
42. McManus MC, Boland ED, Koo HP, Barnes CP, Pawlowski KJ, Wnek GE, et al. Mechanical properties of electrospun fibrinogen structures. Acta Biomater. 2006; 2:19–28. [PubMed: 16701855]
43. Zhang S, Huang Y, Yang X, Mei F, Ma Q, Chen G, et al. Gelatin nanofibrous membrane fabricated by electrospinning of aqueous gelatin solution for guided tissue regeneration. J Biomed Mater Res A. 2009; 90A:671–679. [PubMed: 18563816]
44. Kai D, Prabhakaran MP, Jin G, Ramakrishna S. Guided orientation of cardiomyocytes on electrospun aligned nanofibers for cardiac tissue engineering. J Biomed Mater Res Part B Appl Biomater. 2011; 98B:379–386. [PubMed: 21681953]
45. Prabhakaran MP, Kai D, Ghasemi-Mobarakeh L, Ramakrishna S. Electrospun biocomposite nanofibrous patch for cardiac tissue engineering. Biomed Mater. 2011; 6:055001. [PubMed: 21813957]
46. Ma PX, Zhang RY. Synthetic nano-scale fibrous extracellular matrix. J Biomed Mater Res. 1999; 46:60–72. [PubMed: 10357136]
47. Martinelli V, Cellot G, Toma FM, Long CS, Caldwell JH, Zentilin L, et al. Carbon nanotubes instruct physiological growth and functionally mature syncytia: nongenetic engineering of cardiac myocytes. ACS Nano. 2013; 7:5746–5756. [PubMed: 23734857]

48. Vunjak-Novakovic G, Tandon N, Godier A, Maidhof R, Marsano A, Martens TP, et al. Challenges in cardiac tissue engineering. Tissue Eng Part B Rev. 2010; 16:169–187. [PubMed: 19698068]

49. Jacot JG, McCulloch AD, Omens JH. Substrate stiffness affects the functional maturation of neonatal rat ventricular myocytes. Biophys J. 2008; 95:3479–3487. [PubMed: 18586852]

50. Woo KM, Chen VJ, Ma PX. Nano-fibrous scaffolding architecture selectively enhances protein adsorption contributing to cell attachment. J Biomed Mater Res A. 2003; 67A:531–537. [PubMed: 14566795]

51. Collesi C, Zentilin L, Sinagra G, Giacca M. Notch1 signaling stimulates proliferation of immature cardiomyocytes. J Cell Biol. 2008; 183:117–128. [PubMed: 18824567]

52. Nikkhah M, Edalat F, Manoucheri S, Khademhosseini A. Engineering microscale topographies to control the cell-substrate interface. Biomaterials. 2012; 33:5230–5246. [PubMed: 22521491]

53. Kim HN, Jiao A, Hwang NS, Kim MS, Kang DH, Kim D-H, et al. Nanotopography-guided tissue engineering and regenerative medicine. Adv Drug Deliv Rev. 2013; 65:536–558. [PubMed: 22921841]

54. Schulz R, Heusch G. Connexin 43 and ischemic preconditioning. Cardiovasc Res. 2004; 62:335–344. [PubMed: 15094353]

55. Valarmathi MT, Goodwin RL, Fuseler JW, Davis JM, Yost MJ, Potts JD. A 3-D cardiac muscle construct for exploring adult marrow stem cell based myocardial regeneration. Biomaterials. 2010; 31:3185–3200. [PubMed: 20129663]

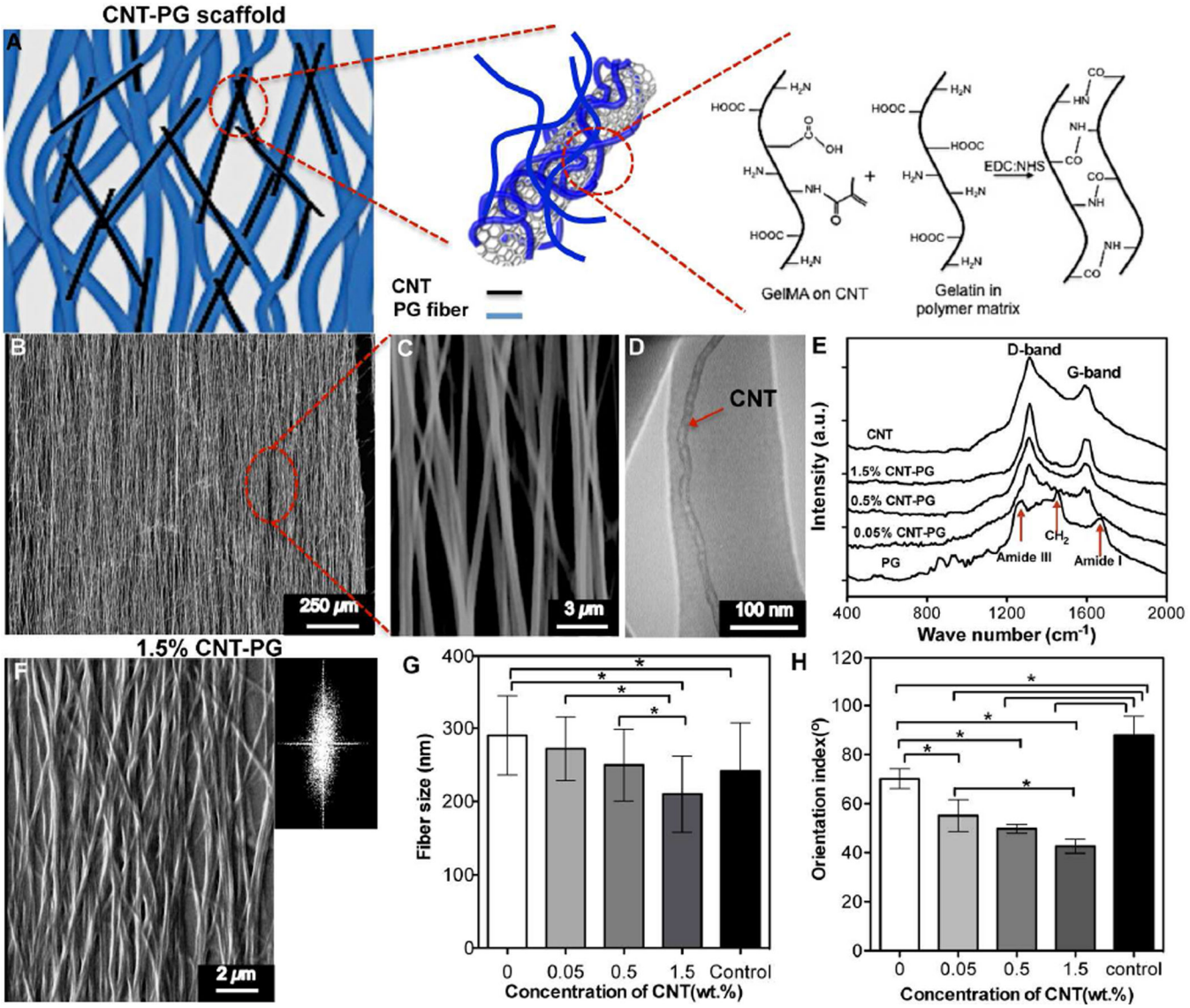

Figure 1.

Structural characteristics of CNT-PG scaffolds. A) Schematic drawing showing the interactions of CNTs with PG scaffold upon crosslinking with EDC/NHS. B and C) SEM images showing uncrosslinked 1.5% CNT-PG scaffold. D) A representative TEM image of 1.5% CNT-PG confirming the well dispersion of CNTs (arrow) aligned along the nanofibers axis. E) Raman spectra of the CNTs and CNT-PG scaffolds. F) SEM and FFT (Inset) images of crosslinked 1.5% CNT-PG. G and H) The average fiber size and orientation index of nanofibrous scaffolds, demonstrating that increasing CNTs content resulted in reduced fiber size and enhanced fiber orientation (random 1.5% CNT-PG scaffold was considered as control) (*: $P<0.05$).

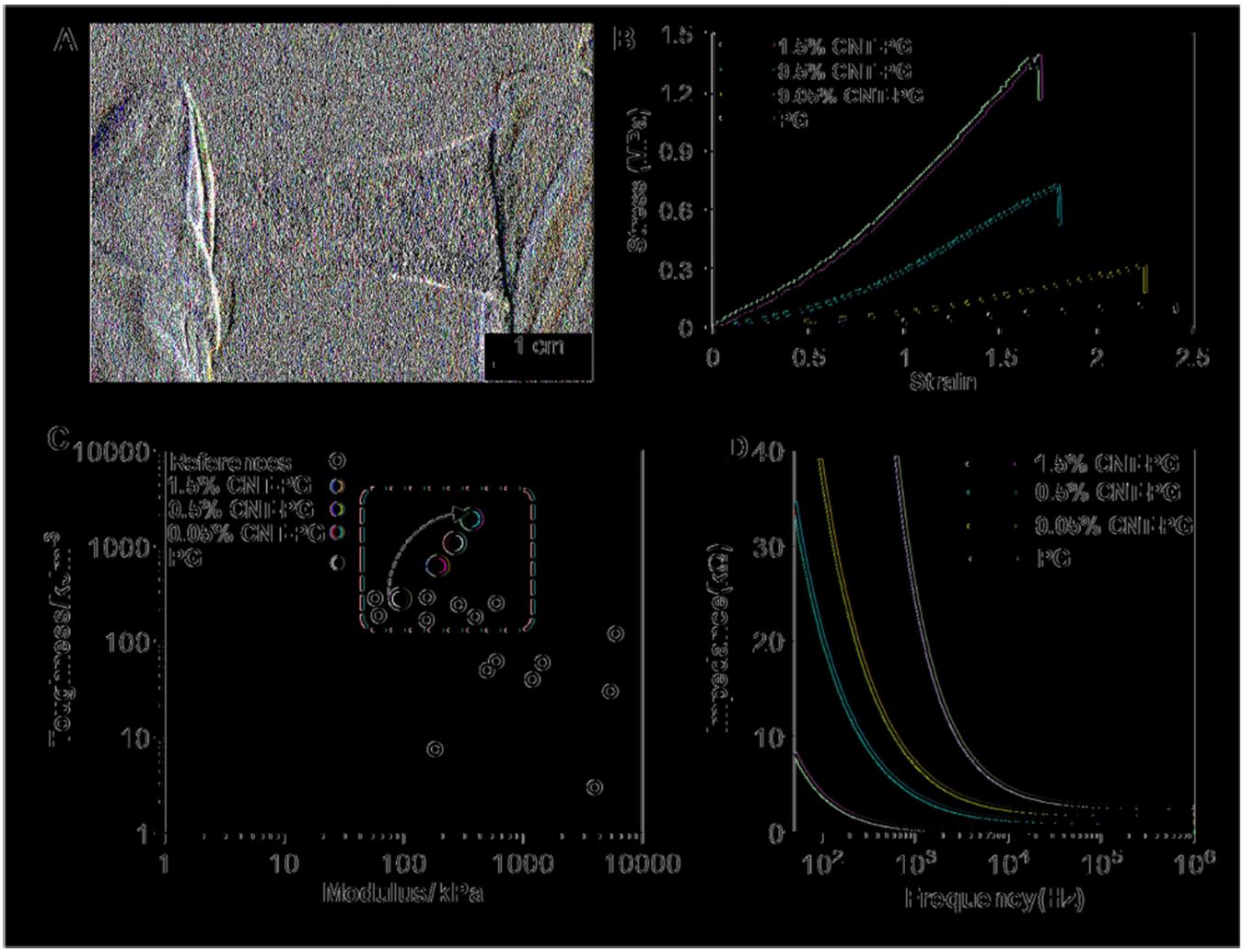

Figure 2.

Physical and electrical characteristics of CNT-PG scaffolds. A) A representative optical image of tough 1.5% CNT-PG scaffold demonstrating easy manipulation of the scaffold. B) Representative stress-strain curves of crosslinked scaffolds after 3 days of soaking in DPBS demonstrating significant improvement in mechanical properties of the scaffolds by increasing the CNT concentration. C) Comparison of the elastic moduli and toughness for previously reported compliant fibrous scaffolds (open circle) [18, 23, 40–46] and the proposed CNT-PG scaffolds consisting of 0% (purple circle), 0.05% (blue circle), 0.5% (red circle) and 1.5% (light green circle for aligned and dark green circle for random nanofibrous scaffolds) CNTs in hydrated state; The dashed window demonstrates the region including the previously developed and the presented CNT-PG tough fibrous scaffolds. As indicated by the arrow, the toughness of the PG scaffolds significantly enhanced through increasing the CNTs concentration. D) The overall impedance of 60μm thick scaffolds as a function of CNTs concentration showing a drastic decrease in impedance through CNTs content.

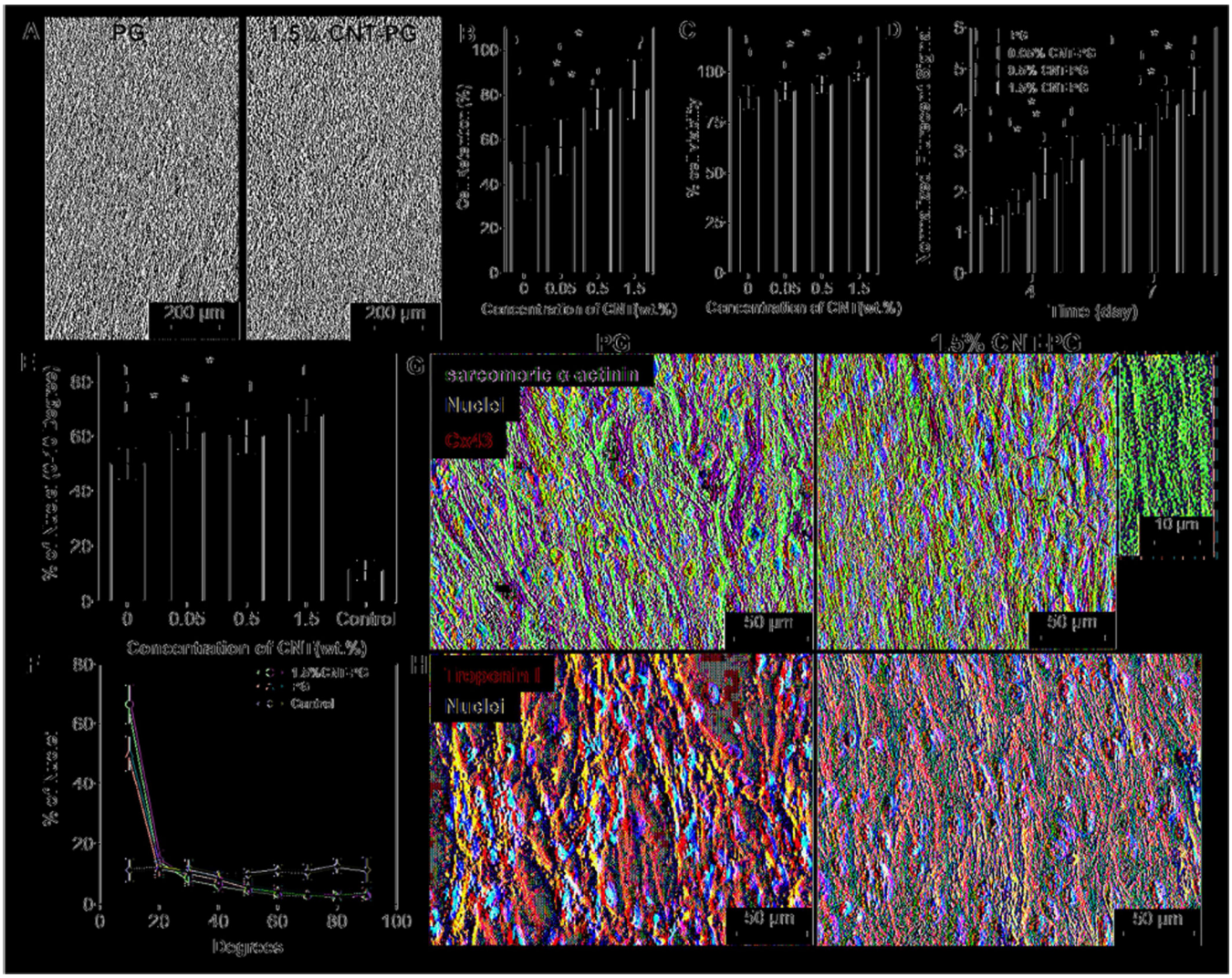

Figure 3.

CM adhesion, viability, metabolic activity, and maturation. A) Phase contrast images of CMs after one day of culture indicating enhanced CMs retention on 1.5% CNT-PG compared to PG scaffold. Quantified results of B) cell retention (day 1), C) live/dead assay (day 1) and D) normalized metabolic activity, confirming significantly improved cell survival and proliferation as a function of CNT content (*: $P < 0.05$). E) Quantified average preferred nuclei alignment between 0–10 degree and F) nuclei alignment distribution on the developed scaffolds after day 7 of culture, indicated significantly enhancement in cellular alignment as a function of CNT content (*: $P < 0.05$) (Random 1.5% CNT-PG scaffold was considered as control). Representative images of CMs proteins expression stained for G) Sarcomeric α-actinin (green), Cx43 (red) and DAPI (blue), and H) Troponin I (red) and DAPI (blue) after 7 days of culture, revealing organized sarcomeres with higher Cx43 expression on 1.5% CNT-PG than PG scaffold. A high magnification image (inset in Fig. 3G) shows interconnected sarcomeric structures perpendicular to the direction of the nanofibers.

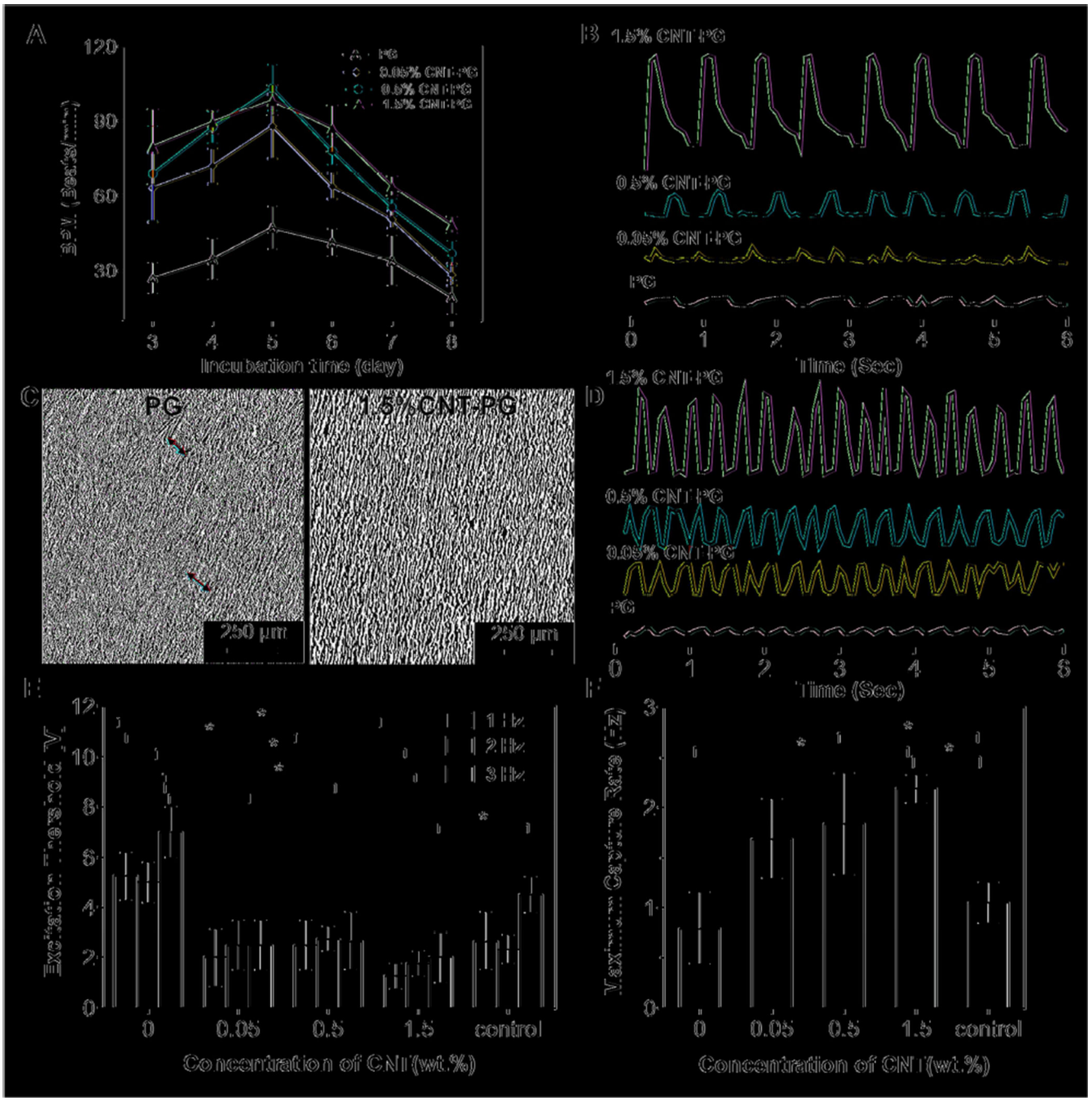

Figure 4.

Electrophysiological functions of engineered cardiac constructs. A) Beating frequency (beats/min, BPM) of constructs as a function of CNT concentration and incubation time. B) Representative spontaneous contraction patterns of CMs cultured on PG scaffolds and CNT incorporated scaffolds recorded after 7 days of cultivation. C) Phase contrast images indicating organized tissue construct and non-continuous aligned tissue (red arrows) on the CNT-PG and PG scaffolds, respectively after 7 days of culture. D) Representative contraction patterns of electrically stimulated CMs on PG scaffold compared to CNT-PG

scaffold after 7 days of culture (Frequency = 1). E) Excitation threshold and F) maximum capture rate of CMs seeded on scaffolds, indicating that increasing the CNT concentration and aligned structures significantly reduced excitation threshold and enhanced maximum capture rate (CMs cultured on random 1.5% CNT-PG scaffold was considered as control). (*:$P<0.05$).